# Supporting Information

# Susceptible Electron Spin Adhering to Yttrium Cluster inside an Azafullerene C$_{79}$N

Yihan Ma,[a,b] Taishan Wang,*[a] Jingyi Wu,[a] Yongqiang Feng,[a] Li Jiang,[a] Chunying Shu[a] and Chunru Wang*[a]

# Contents

**Experimental Section:** Preparation and characterization of Y$_2$@C$_{79}$N and its fulleropyrrolidines

*Figure S1.* MALDI-TOF MS for the toluene extract of the soot containing mostly yttrium endohedral metallofullerenes.

*Figure S2.* Chromatogram of the isolated Y$_2$@C$_{79}$N (20×250 mm Buckyprep-M column; flow rate 12 mL/min; toluene as eluent). The inset shows the MALDI-TOF MS for isolated Y$_2$@C$_{79}$N.

*Figure S3.* HPLC profile of reaction mixture (20×250 mm Buckyprep-M column; flow rate 12 mL/min; toluene as eluent).

*Figure S4.* The first stage HPLC profile of Y$_2$@C$_{79}$N fulleropyrrolidine mono-adducts (20×250 mm Buckyprep column; flow rate 6 mL/min; toluene as eluent).

*Figure S5.* The second stage HPLC profile of Y$_2$@C$_{79}$N fulleropyrrolidine mono-adducts (20×250 mm Buckyprep-M column; flow rate 3 mL/min; toluene as eluent)

*Figure S6.* Chromatogram of the isolated Y$_2$@C$_{79}$N fulleropyrrolidine mono-adduc isomer **A**，**B** and **C** (20×250 mm Buckyprep column; flow rate 3mL/min; toluene as eluent).

*Figure S7.* UV-Vis absorption spectra of Y$_2$@C$_{79}$N pristine and its fulleropyrrolidine mono-adducts A，B and C in toluene.

*Figure S8.* EPR spectrum of Y$_2$@C$_{79}$N fulleropyrrolidine mono-adducts C measured in CS$_2$ solution at 298 K.

**Theoretical calculation Section:**

*Table S1.* Energies of sixty-two Y$_2$@C$_{79}$N fulleropyrrolidine mono-adducts
*Table S2.* Energies of three Y$_2$@C$_{79}$N fulleropyrrolidine mono-adducts with different addend orientation
*Figure S9.* The calculated spin density distributions Y$_2$@C$_{79}$N fulleropyrrolidine mono–adducts. The blue area presents the unpaired spin.

*Experimental Section:*

   Graphite rods were core-drilled and subsequently packed with a mixture of Y/Ni$_2$ alloy and graphite powder in a weight ratio of 2:1. These rods were then vaporized in a Krätschmer-Huffman generator at 192 Torr He and 8 Torr N$_2$. The resulting soot was Soxlet-extracted with toluene for 12 h. Y$_2$@C$_{79}$N was isolated from various empty fullerenes and other yttrium metallofullerenes by multi-stage HPLC.

   The synthesis of Y$_2$@C$_{79}$N fulleropyrrolidines was carried out in *o*-dichlorobenzene solution of pure Y$_2$@C$_{79}$N with N-ethylglycine and 4-Diphenylaminobenzaldehyde at 393 K for 30 min. The products was isolated and purified by HPLC. The ESR experiments were performed on Bruker E-500 EPR spectrometer after removing oxygen by bubbling nitrogen. The EPR spectrometer utilizes a microwave frequency of 9.77 GHz for ESR experiment at 298 K and 9.52 GHz for ESR experiment at 153 K.

*1.*   **The synthesis and purification of Y$_2$@C$_{79}$N.**
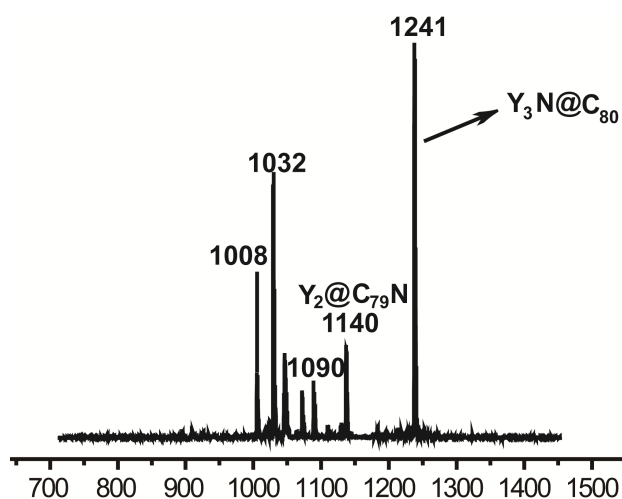


**Figure S1**. MALDI-TOF MS for the toluene extract of the soot containing mostly yttrium endohedral metallofullerenes.
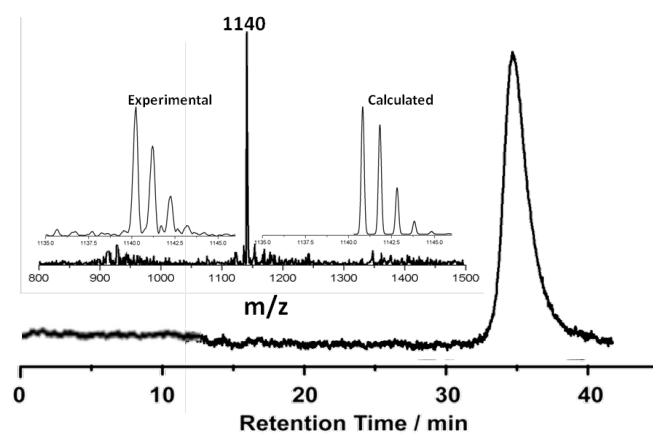


**Figure S2**. Chromatogram of the isolated Y$_2$@C$_{79}$N (20×250 mm Buckyprep-M column; flow rate 12 mL/min; toluene as eluent). The inset shows the MALDI-TOF MS for isolated Y$_2$@C$_{79}$N.

## 2. The synthesis and purification of $Y_2@C_{79}N$ fulleropyrrolidines

The synthesis of $Y_2@C_{79}N$ fulleropyrrolidines was carried out in *o*-dichlorobenzene solution of pure $Y_2@C_{79}N$ with N-ethylglycine and 4-Diphenylaminobenzaldehyde at 120 ℃ for 30 min. The products were isolated and purified by high performance liquid chromatography (HPLC).
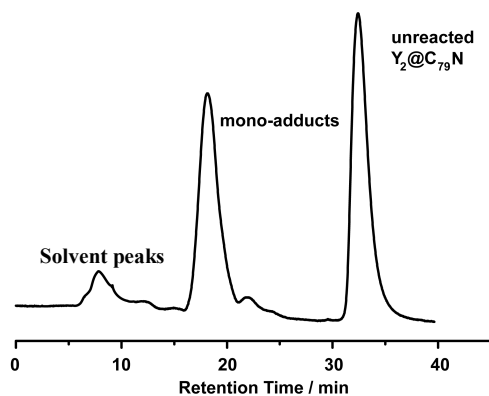


**Figure S3.** HPLC profile of reaction mixture (20×250 mm Buckyprep-M column; flow rate 12 mL/min; toluene as eluent).

## 3. HPLC data of purified $Y_2@C_{79}N$ fulleropyrrolidine mono-adducts

The stage 1 and 2 separations were executed to obtain purified $Y_2@C_{79}N$ fulleropyrrolidine mono-adducts. Figure S3 and Figure S4 show the HPLC data of purified $Y_2@C_{79}N$ fulleropyrrolidine mono-adduct isomer **A**, **B** and **C** and with Buckyprep columns.
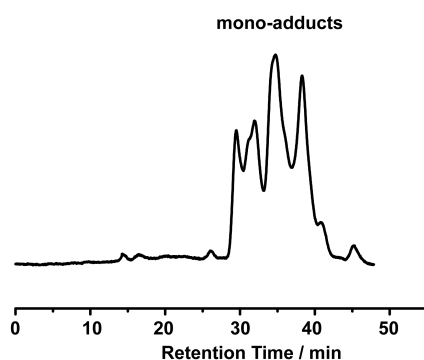


**Figure S4.** The first stage HPLC profile of $Y_2@C_{79}N$ fulleropyrrolidine mono-adducts (20×250 mm Buckyprep column; flow rate 6 mL/min; toluene as eluent).
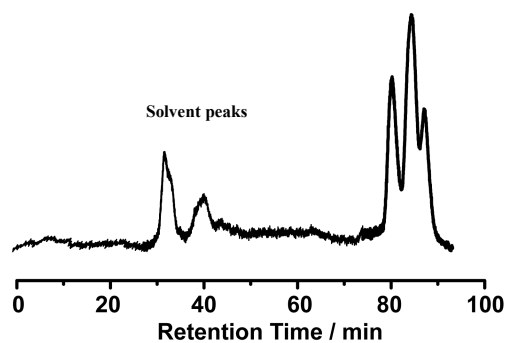
**Figure S5.** The second stage HPLC profile of $Y_2@C_{79}N$ fulleropyrrolidine mono-adducts (20×250 mm Buckyprep-M column; flow rate 3 mL/min; toluene as eluent)
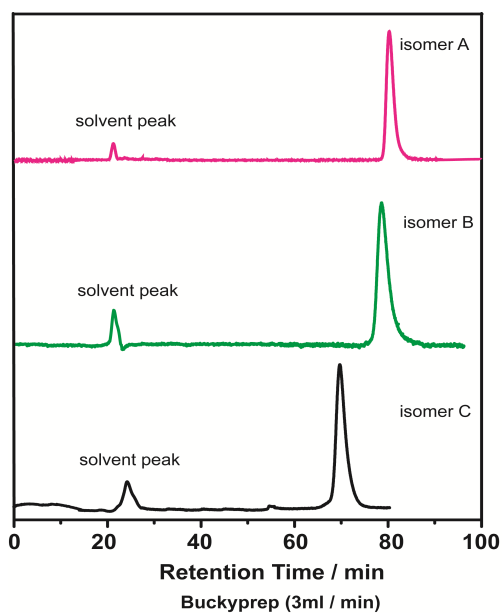


**Figure S6.** Chromatogram of the isolated $Y_2@C_{79}N$ fulleropyrrolidine mono-adduc isomer **A**，**B** and **C** (20×250 mm Buckyprep column; flow rate 3mL/min; toluene as eluent).
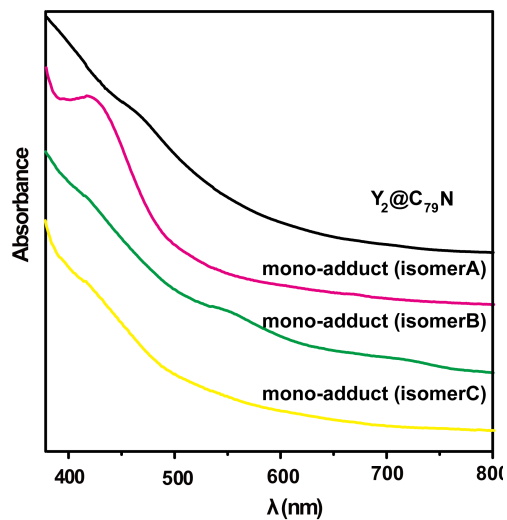


**Figure S7.** UV-Vis absorption spectra of $Y_2@C_{79}N$ pristine and its fulleropyrrolidine mono-adducts A，B and C in toluene.

## 5. EPR spectrum of $Y_2@C_{79}N$ fulleropyrrolidine mono-adducts C.

Figure S7 presents the experimental ESR spectrum of $Y_2@C_{79}N$ fulleropyrrolidine mono-adduct isomers **C,** which possesses nearly identical paramagnetic performance with isomer B.
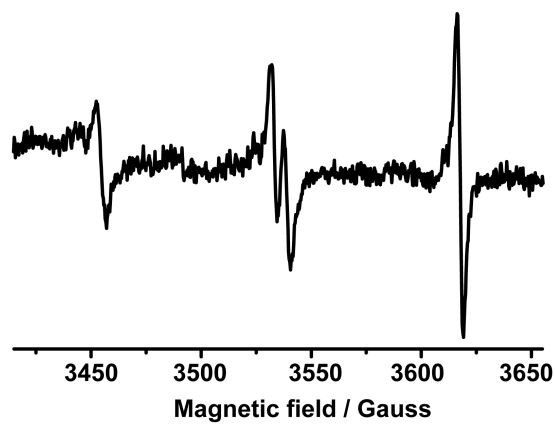


***Figure S8.*** EPR spectrum of $Y_2@C_{79}N$ fulleropyrrolidine mono-adducts C measured in $CS_2$ solution at 298 K.

### Theoretical calculation Section:

Density functional theory (DFT) calculations were preformed to study the energies of sixty-two $Y_2@C_{79}N$ fulleropyrrolidine mono-adducts. And the possible reaction sites were listed according to the calculations.

**Table S1.** Energies of sixty-two $Y_2@C_{79}N$ fulleropyrrolidine mono-adducts

| Mono-adducts | $\Delta E$ (kcal/mol) |
|---|---|
| isomer 17 | 0.000 |
| isomer 19 | 0.212 |
| isomer 11 | 1.088 |
| isomer 8 | 1.567 |
| isomer 15 | 1.942 |
| isomer 16 | 2.231 |
| isomer 2 | 2.256 |
| isomer 14 | 2.528 |
| isomer 7 | 2.547 |
| isomer 5 | 2.907 |
| isomer 20 | 3.123 |
| isomer 6 | 3.229 |
| isomer 23 | 3.488 |
| isomer 13 | 3.562 |
| isomer 21 | 3.705 |
| isomer 31 | 4.445 |
| isomer 4 | 5.911 |
| isomer 53 | 6.414 |
| isomer 33 | 6.672 |
| isomer 59 | 6.871 |
| isomer 24 | 7.036 |
| isomer 45 | 7.040 |
| isomer 55 | 7.135 |
| isomer 50 | 7.603 |
| isomer 62 | 8.250 |
| isomer 35 | 8.804 |
| isomer 26 | 9.103 |
| isomer 10 | 9.233 |
| isomer 9 | 9.263 |
| isomer 46 | 9.264 |
| isomer 29 | 9.348 |
| isomer 30 | 9.348 |
| isomer 28 | 9.886 |
| isomer 42 | 10.301 |
| isomer 39 | 10.384 |
| isomer 43 | 10.403 |
| isomer 27 | 10.584 |

| | |
|---|---|
| isomer 12 | 10.612 |
| isomer 47 | 10.785 |
| isomer 44 | 10.838 |
| isomer 25 | 10.888 |
| isomer 61 | 11.053 |
| isomer 56 | 11.091 |
| isomer 48 | 11.315 |
| isomer 1 | 11.620 |
| isomer 22 | 11.759 |
| isomer 49 | 12.012 |
| isomer 52 | 12.023 |
| isomer 51 | 12.251 |
| isomer 3 | 13.158 |
| isomer 34 | 13.561 |
| isomer 40 | 13.925 |
| isomer 41 | 13.925 |
| isomer 18 | 13.937 |
| isomer 32 | 14.260 |
| isomer 54 | 14.569 |
| isomer 60 | 15.039 |
| isomer 57 | 17.701 |
| isomer 58 | 19.580 |
| isomer 37 | 22.680 |
| isomer 38 | 22.861 |
| isomer 36 | 22.861 |

Theoretical calculations were also executed to disclose the influence of addend orientation on the relative stability and also on the spin localization. And the results showed that the addend orientation has no effect on relative stability as well as spin distributions.

*Table S2.* Energies of Energies of three $Y_2@C_{79}N$ fulleropyrrolidine mono-adducts with different addend orientation

| Mono-adducts | $\Delta E$ (kcal/mol) |
|---|---|
| isomer 17 | 0.000 |
| isomer 17-trans | 2.787 |
| isomer 19 | 0.212 |
| isomer 19-trans | 0.497 |
| isomer 11 | 1.088 |
| isomer 11-trans | 1.236 |

**mono-adduct**
**(isomer 17- trans)**

**mono-adduct**
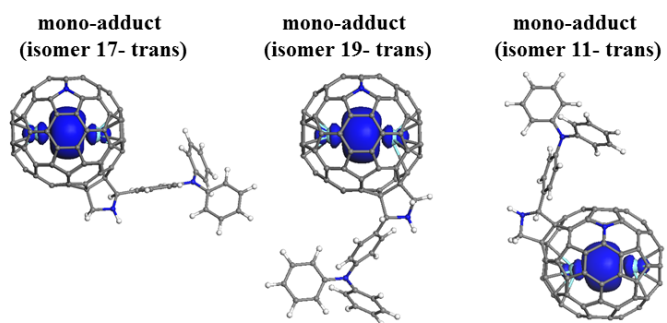**(isomer 19- trans)**

**mono-adduct**
**(isomer 11- trans)**



*Figure S9.* The calculated spin density distributions $Y_2@C_{79}N$ fulleropyrrolidine mono–adducts. The blue area presents the unpaired spin.